Inorganic Chemistry Research

Article

Co-precipitation Synthesis of α-Fe_2O_3: Characterization and Their Activities on Photocatalytic Degradation of Methylene Blue

Aliakbar Dehno Khalaji*, Emad Jafari

Department of Chemistry, Faculty of Science, Golestan University, Gorgan, Iran

Received: November 6, 2023; Accepted: January 6, 2024

Cite This: *Inorg. Chem. Res.* **2023**, *7*, 27-33. DOI: 10.22036/j10.22036.2024.424174.1155

Abstract: In this work, spherical α-Fe_2O_3 were synthesized using the facile co-precipitation followed by calcination at 500 °C (Fe-1) and 700 °C (Fe-2) for 3 h. The as-synthesized Fe-1 and Fe-2 samples were characterized by Fourier-transform Infrared (FT-IR) spectroscopy, X-ray powder diffraction (XRD), vibrating sample magnetometer (VSM) and transmission electron microscope (TEM). All results predict the successful preparation of Fe-1 and Fe-2 as soft magnetic materials. In addition, the photocatalytic activity of as-synthesized Fe-1 and Fe-2 were evaluated by degrading methylene blue (MB) dye is aqueous solution under simulated sunlight irradiation at low alkaline pH in the presence of a small amount of H_2O_2 as an oxidant. The effects of the initial pH of the solution and irradiation time on the photocatalytic properties were investigated. Under the best optimized conditions, Fe-1 exhibited better MB degradation with 94% efficiency than Fe-2 (78%). The kinetic study showed that the photocatalytic degradation of MB was followed by a pseudo first-order (PFO) model. The reusability studies of the samples predicted good stability and efficiency after 6 cycles.

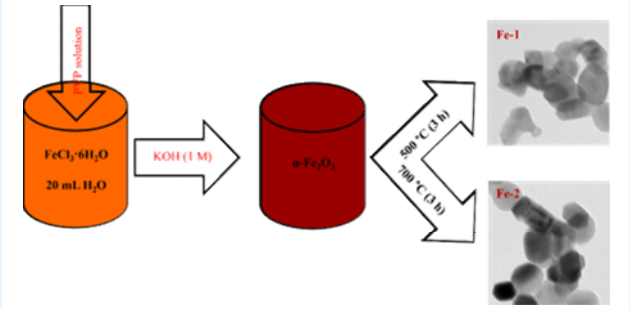

Keywords: Spherical α-Fe_2O_3, Photocatalytic, Degradation, Methylene blue

1. INTRODUCTION

In recent years, one of the important challenges for human life is environmental pollutions by various organic dyes such as methyl orange,[1,2] bisphenol A,[3] congo red,[4,5] rhodamine B,[6-9] bromo green,[2] methyl red,[2] crystal violet[10] and methylene blue[1,2,10-19] used in different factories. The organic dyes have complex structure containing azo, aromatic, cationic and anionic groups which are very stable in environment, soluble in water, toxic and potentially mutagenic and carcinogenic and finally reduces the photosynthetic reactions due to inhibit sunlight penetration.[1-7] Therefore, removal of organic dye from environment is necessary. Until now, different techniques such as reverse osmosis, membrane technology, physical adsorption, biological, filtration, flocculation[20-25] and photocatalytic degradation[1-18] are the processes of pollution removal from wastewaters. From them, photodegradation of different organic dyes using different shapes of α-Fe_2O_3 has great attention[1-3,5-7,10,18,26,27] and is among the promising technology owing to its low-cost, low energy utilization, excellent catalytic activity, include mild reaction condition, and its capability of consuming renewable solar energy.[28] Until now, Various shapes of hematite α-Fe_2O_3 have been prepared and attracted considerable attention to many researchers owing to their capability to photocatalytic degradation of different organic dyes under UV/visible light irradiation.[1-3,5-7,10,18,26-28] α-Fe_2O_3 is an n-type semiconductor with the narrow band gap of ≈ 2.2 eV,[1] known as good candidate to adsorb UV and Visible light and can be used as an efficient photocatalyst for photodegradation of organic dyes.[1-3,5-7] Previous results confirmed that the crystalline size, shape and also surface area of α-Fe_2O_3 are very important for the photodegradation of different organic dyes.[6,7,28] Therefore, many researchers' effort to prepared new α-Fe_2O_3 with different shape, size and surface area.[1-3,5-7,10,18] For example, Weldegebrieal et al.[1] prepared α-Fe_2O_3 nanoparticles by biosynthesis route for application as new photocatalyst to photodegradation of methylene blue and methyl orange dyes at alkaline pH under sunlight irradiation. Rhombohedral α-Fe_2O_3 nanoparticles has been successfully synthesized by Ye et al.[3] as an efficient photocatalyst in photocatalytic degradation of bisphenol

A[9]. Kusior et al.[6] was synthesized different shapes of α-Fe_2O_3 nanoparticles *via* an ion-mediated hydrothermal route to photodegradation of rhodamine B. Gupta et al.[2] reported fast photodegradation of methylene blue (95%), bromo green (94%), methyl red (76%) and methyl orange (94%) within 5 min in 32 W UV/H_2O_2 system using as-prepared coral-like α-Fe_2O_3 nanoparticles by surfactant-mediated simple co-precipitation-oxidation route. Khurram et al.[5] showed high-efficient degradation of congo red dye (98.9%) using α-Fe_2O_3based nanocomposites in 60 min under visible light. Qiu et al.[7] reported high photodegradation (99%) of RhB using as-prepared hollow polyhedral α-Fe_2O_3 nanoparticles under visible light/H_2O_2 system. α-Fe_2O_3 nanofibers prepared by Arauji et al.[10] and used as photodegradation of methylene blue, 66 and 48%, under visible and UV light irradiation after 5 h. These works showed that the morphology of α-Fe_2O_3 nanoparticles greatly influences the photodegradation performance.[10,18] Even though α-Fe_2O_3 photocatalysis has great attention in degradation of organic dyes, it remains a challenge to prepared high-efficient α-Fe_2O_3 photocatalyst.

In this work, in continuation of our previous works,[29,30] we aimed to explore the effects of calcination temperature on morphology, magnetic properties, and their photocatalytic activity of as-synthesized α-Fe_2O_3.

2. EXPERIMENTAL

Material and methods

$FeCl_3{\cdot}6H_2O$ as iron precursor, polyvinylpyrrolidone (PVP), KOH, H_2O_2 and MB were purchased and used as received without any further purification. Fourier Transform Infra-Red spectra of α-Fe_2O_3 nanoparticles were recorded using NICOLET IR200 FT-IR spectrophotometer in KBr pellets from 4000 to 400 cm^{-1}. XRD patterns were performed using a PANalytical's X'pert system by Cu *kα* radiation at scan range of $10° < 2\theta < 80°$. The magnetic properties of the as-synthesized α-Fe_2O_3 nanoparticles were recorded by the American Lake Shore VSM 7307 vibration sample magnetometer (VSM). Transmission electron microscopy (TEM) image were recorded on a FEI Tecnai G2 f20 microscope. The Ultraviolet-Visible absorption of MB dye solution at over time were recorded on a Shimadzu UV-3101 PC UV-Vis spectrophotometer.

Preparation of α-Fe_2O_3 (Fe-1 and Fe-2)

To an aqueous solution of $FeCl_3{\cdot}6H_2O$ (0.01 mmol in 20 mL), was added a solution of PVP (15 w/v, 10 mL) and vigorously stirred for about 30 min. After that, an aqueous solution of KOH (1 M) was added dropwise under magnetic stirring until the pH solution was achieved to 12. After stirring for 10 h at 80 °C, the brown precipitates were filtered, washed with deionized water three times, and dried at 80 °C for 12 h. The dried brown precipitates were calcined at 500 °C and 700 °C for 3 h. The obtained dark red precipitates (Fe-1 and Fe-2) were washed, dried and characterized.

Photocatalytic experiments

All the photocatalytic experiments were performed at room temperature by the photocatalytic reactor which consisted of a reaction beaker and a Xe lamp positioned vertically to the beaker. Typically, to a 50 mL of MB solution (25 mg/L) in a 100 mL glass tube was added the suitable amount of photocatalysts Fe-1 and/or Fe-2. The mixture was magnetically stirred at the speed of 500 rpm for 30 min in the dark to achieve an adsorption/desorption equilibrium between the MB dye and α-Fe_2O_3 catalysts. Then, 3 mL of H_2O_2 was added to improved catalyst efficiency and the suspension was exposed to simulated sunlight (high-pressure Xe lamp, 300 w) for 150 min. After a given time intervals, 3 mL of suspension was collected and the catalysts in the solution were removed using a centrifuge. Afterwards, the content of MB dye was analyzed using UV-Vis spectrophotometer at λ_{max} of 664 nm. For the reusing tests, the samples were recovered after centrifuged, washed with alkaline solution and subsequently dried at 80°C for 3 h. The photodegradation efficiency (%) of MB was calculated using the following equation where C_o and C_t are MB concentration at initial and over time, respectively.

$$R\ (\%) = \frac{(Co - Ct)}{Co} \times 100 \qquad (1)$$

3. RESULTS AND DISCUSSION

Synthesis

To date, various shapes of α-Fe_2O_3 have been prepared using different techniques such as solvothermal,[31,32] hydrothermal,[34-37] thermal decomposition,[30] green chemistry,[1,38] sol-gel,[39] co-precipitation,[2,40] solution blow spinning,[10] and p123 soft template assisted.[3] From them, co-precipitation accompanied thermal decomposition is the best routes for preparation of different metal oxide nanoparticles because of it is low-cost, simple and convenient method.[29,30,35,41-47]

Characterization

FT-IR spectroscopy was used to identify the surface types of functional groups available in the as-prepared Fe-1 and Fe-2 nanoparticles. Figure 1 shows a typical FT-IR spectra of Fe-1 and Fe-2 samples prepared at 500 and 700 °C, respectively. The broad and weak absorption peaks at ≈ 3430 and 1640 cm^{-1} corresponded to the O-H vibration of H_2O molecules physically adsorbed on the

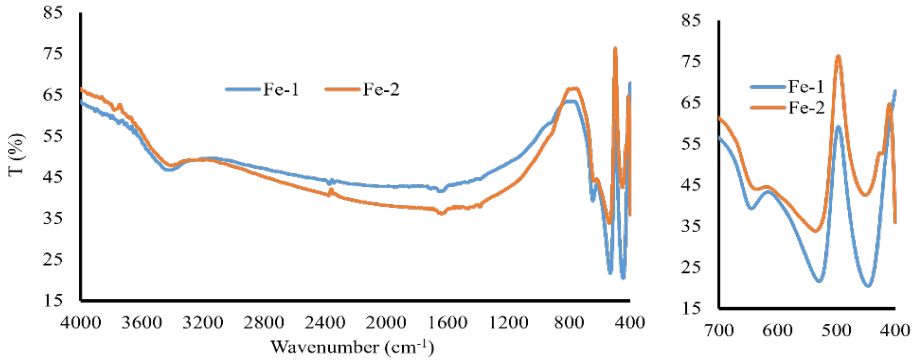

Figure 1. FT-IR spectra of α-Fe_2O_3 nanoparticles Fe-1 and Fe-2.

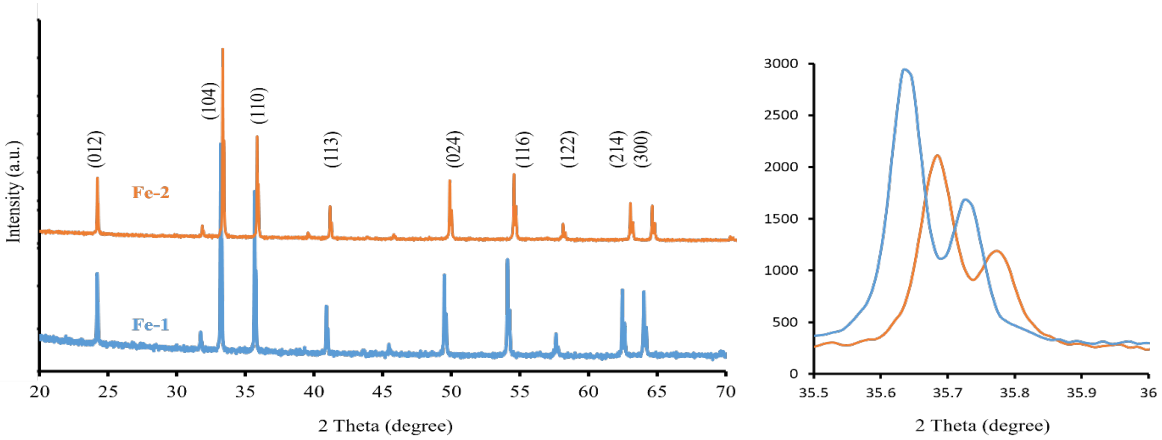

Figure 2. XRD patterns of Fe-1 and Fe-2.

surface of particles.[1,2,18] In addition, the three sharp peaks appeared at ≈ 445, 530, and 645 cm^{-1} are ascribed to the Fe-O vibration bonds as characteristic peaks of α-Fe_2O_3. [1,2,7,18,29,30,34,35,40]

The XRD patterns of the as-prepared Fe-1 and Fe-2 samples are shown in Figure 2, predicted that all characteristic peaks observed at 2θ values of 24.15 (012), 33.15 (104), 35.65 (110), 40.87 (113), 49.45 (024), 54.82 (116), 57.63 (112), 62.45 (214) and 64.01 (300) are well matched with the standard card of rhombohedral structure (JCPDS no. 33-0664) of pure hematite α-Fe_2O_3 with cell parameters of a = b = 5.036 Å, and c = 13.749 Å.[1-3,5-7,10,18,29,30,34,35,40] Using Debye-Scherrer equation according the maximum intensity peak at 33.15° corresponding to (104) plane, D = 0.9 λ / β cosθ, where λ is the X-ray wavelength, β is the line broadening at half of the maximum intensity and θ is the diffraction angle,[10] the average crystalline sizes of particles was calculated about 28.3 nm for Fe-1 and 25.8 nm for Fe-2 are close to those values from TEM images (Figure 3).

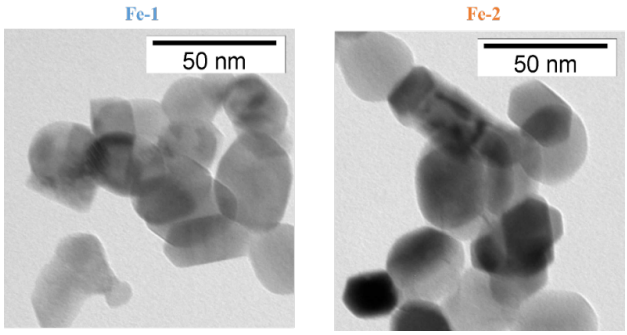

Figure 3. TEM images of Fe-1 and Fe-2.

The morphology of the as-synthesized α-Fe_2O_3 was characterized by the transmission electron microscope (TEM) were shown in Figure 3. It can be seen that the samples Fe-1 and Fe-2 presented the quasi-spherical shapes, with smaller sizes of < 100 nm with small aggregation.

Figure 4 shows magnetic hysteresis loops of samples (Fe-1 and Fe-2) at room temperature. VSM curves exhibit the ferromagnetic behavior of Fe-1 and Fe-2 nanoparticles with M_s of 4.69 and 7.41 emu/g, respectively. Also, the

samples have no hysteresis loops and H_c (coercivity field) and also M_r (remanent magnetization) are very small. This value is larger than the reported 0.78 emu/g for α-Fe_2O_3 fibers.[10,48-50]

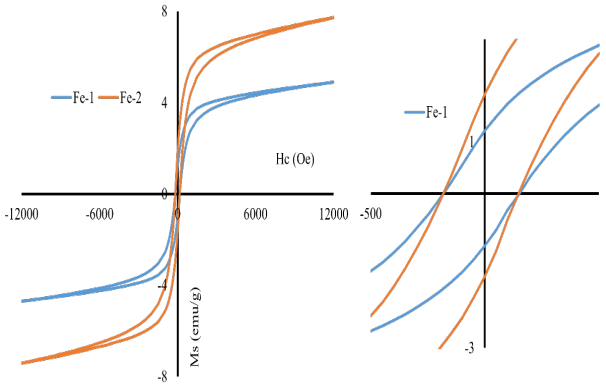

Figure 4. VSM curves of Fe-1 and Fe-2.

At ambient conditions, the surface of α-Fe_2O_3 can be exposed to hydroxyl as a functional group, which corresponds to the adsorption/desorption of organic dyes.[6,51-53] The isoelectric point of Fe-1 and Fe-2 in aqueous solution almost equal and calculated at pH of 8.7 (Figure 5), similar to previous reports for hematite.[6] Under this pH, the surface of samples has positive charge due to the formation of $FeOH_2^+$ groups, and at pH > 8.7, the surface of samples become negative due to the increases of FeO^- groups.[6] The values of zeta potential are sensitive to temperature, and impurities.

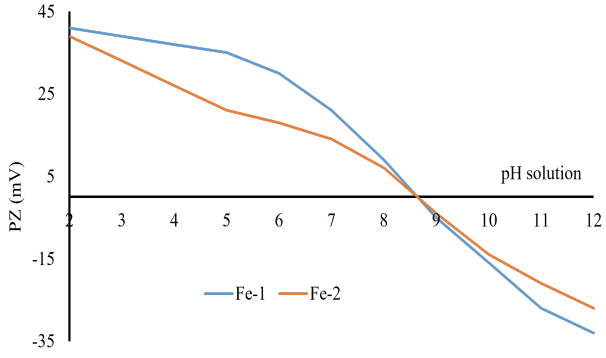

Figure 5. The zeta potential of Fe-1 and Fe-2 samples at 200 °C for 16 h.

MB Photodegradation studies

At different pH, the hydroxyl groups on the surface of Fe-1 and Fe-2, can be adsorbed or desorbed H^+ ions and resulted to formation $FeOH_2^+$ or FeO^- groups.[6] Then, the effect of different pH solution (3, 5, 7, 9, and 11) was studied for photodegradation of MB (Fig. 6). As can be seen in Figure 6, high efficiency of MB degradation was observed at pH value of 9 at the presence of 0.03 g of catalyst, because of MB molecules easy adsorbed by Fe-1 and Fe-2 samples due to the good electrostatic attractions between the negative surface charge of Fe-1 and Fe-2 samples and positive charge of MB molecules. Then pH solution of 9 was selected for investigation of irradiation time on photodegradation of MB.

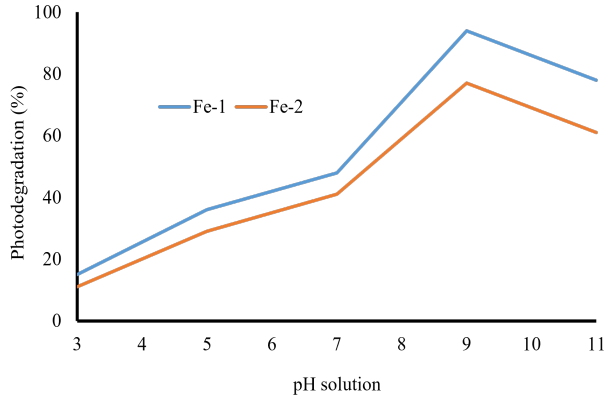

Figure 6. The effect of pH solution on the photocatalytic degradation of MB.

Figure 7 represented the effect of irradiation time on the photodegradation efficiency of MB dye using 0.03 g of Fe-1, and Fe-2 as photocatalyst. As can be seen in Figure 7, the degradation activity decreased in the following order: Fe-2 < Fe-1, predict the photodegradation activity increased with small size of Fe_2O_3. After visible light irradiation for 150 min, the photodegradation of MB using Fe-1 reached 94%, is much higher than photodegradation of MB using Fe-2 (77%), because of the difference in crystal size. In comparison to the other photocatalyst for MB degradation, Fe-1 shows a better efficiency in photodegradation of MB under visible light irradiation (Table 1).

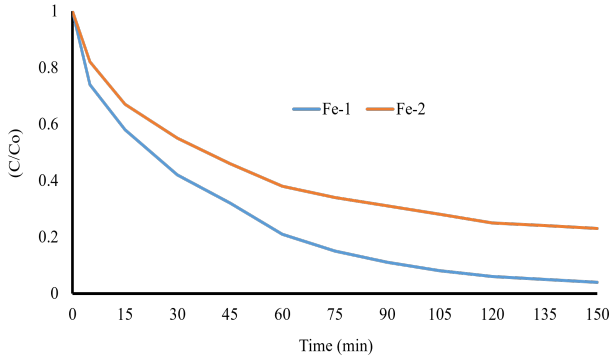

Figure 7. The effect of irradiation time on photocatalytic degradation of MB.

The MB photodegradation using as-synthesized Fe_2O_3 was investigated using the simplified Langmuir kinetic model (Figure 8), and followed by pseudo first order kinetic model.[1-3,6,7]

$$\ln(C_t/C_o) = -k_1 t$$

Proposed reaction mechanism of MB degradation in the presence of H_2O_2 (as electron trap) and Fe_2O_3 nanoparticles (as absorption of visible light) is explained as follow equations:[1-3,6,7]

$$Fe_2O_3 + h\nu \rightarrow h^+_{VB} + e^-_{CB}$$
$$e^-_{CB} + O_2 \rightarrow O_2^{-\circ}$$
$$H_2O_2 + e^-_{CB} \rightarrow OH^\circ + OH^-$$
$$O_2^{-\circ} + H_2O \rightarrow HO_2^\circ + OH^-$$
$$HO_2^\circ + H_2O \rightarrow OH^\circ + H_2O_2$$
$$MB + OH^\circ \rightarrow \text{Degraded products}$$

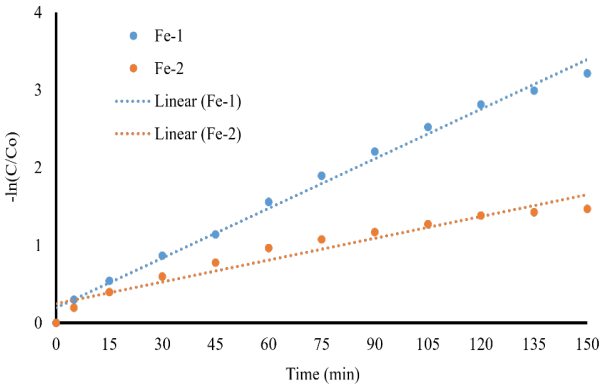

Figure 8. The pseudo first order kinetics of MB photodegradation.

Table 1. Comparison of MB photodegradation using Fe-1 and Fe-2 and other photocatalyst

Catalyst	Conditions	% of MB	Ref.
Biosynthesized α-Fe_2O_3 nanoparticles	UV/H_2O_2/90 min	94.7	1
Co doped α-Fe_2O_3 nanoparticles	UV/120 min	92	18
α-Fe_2O_3 nano fibers	Visible/5 h	66	10
α-Fe_2O_3 nanofibers	UV/5 h	48	10
Coral-like α-Fe_2O_3 nanoparticles	UV/H2O2/75 min	95	2
CeO_2 nanoparticles	UV/120 min	96	12
Cubic CeO_2 nanoparticles	UV/180 min	70	13
CeO_2 nanoparticles	UV/75 min	85	14
CeO_2 nanoparticles	Visible/70 min	99	16
CeO_2 nanoparticles	UV/120 min	96	11
Fe-1	Visible/150 min	94	This work
Fe-2	Visible150 min	78	This work

The reusability of Fe-1 and Fe-2 samples in photodegradation of MB studied after six times recycling process and represented in Figure 9. No significant loss of photocatalytic activity of samples was observed, predicted that the stability of the samples.[1,7]

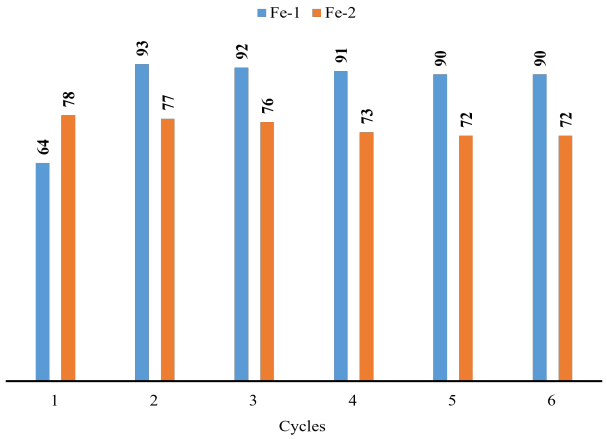

Figure 9. Recyclability of Fe-1 and Fe-2 for MB photodegradation in aqueous solution.

4. CONCLUSIONS

In summary, spherical α-Fe_2O_3 was synthesized using the facile PVP-assisted co-precipitation followed by calcination, characterized and the photocatalytic activity of them was studied by degradation of methylene blue under visible light irradiation in the presence of a small amount of H_2O_2. The results predicted that the Fe-1 sample exhibited better MB degradation with 94% efficiency than Fe-2 sample (78%), because of difference crystal sizes. The samples remain stable with good efficiency even after 6 cycle's times, which is favorable for the potential application in photodegradation of organic dyes.

CONFLICTS OF INTEREST

The authors declare that they have no conflict of interest.

ACKNOWLEDGMENTS

We would like to thank the Golestan University.

AUTHOR INFORMATION

Corresponding Author

Aliakbar Dehno Khalaji: Email: alidkhalaji@yahoo.com, *ORCID*: 0000-0002-8362-5158

Author

Emad Jafari

REFERENCES

1. G. K. Weldegebrieal, A. K. Sibhatu, *Optik* **2021**, *241*, 167226.

2. N. K. Gupta, Y. Ghaffari, J. Bae, K. S. Kim, *J. Mol. Liq.* **2020**, *301*, 112473.
3. C. Ye, K. Hu, Z. Niu, Y. Lu, L. Zhang, K. Yan, *J. Water Process Eng.* **2019**, *27*, 205-210.
4. S. Gnanam, V. Rajendran, *J. All. Compd.* **2018**, *735*, 1854-1862.
5. R. Khurram, Z. Wang, M.F. Ehsan, *Environ. Sci. Poll. Res.* **2021**, *28*, 17697-17711.
6. A. Kusior, K. Michalec, P. Jelen, M. Radecka, *Appl. Surf. Sci.* **2019**, *476*, 342-352.
7. M. Qiu, R. Wang, X. Qi, *J. Tiwan Inst. Chem. Eng.* **2019**, *102*, 394-402.
8. J. Malleshappa, H. Nagabhushana, S. C. Sharma, Y. S. Vidya, K. S. Anantharaju, S. C. Prashantha, B. Daruka Prasad, H. Raja Naika, K. Lingaraju, B. S. Surendra, *Spectrochim. Acta A* **2015**, *149*, 452-462.
9. K. K. A. Becker, A. Bloesser, T. Weller, J. Yimm, C. Suchomski, R. Marschall, *J. Phys. Chem. C* **2017**, *121*, 27126-27138.
10. R. N. Araujo, E. P. Nascimento, H. C. T. Firmino, D. A. Macedo, G. A. Neves, M. A. Morales, R. R. Menezes, *J. All. Compd.* **2021**, *882*, 160683.
11. S. A. Jasim, P. Machek, W. K. Abdelbasset, M. Jarosova, H. S. Majdi, A. D. Khalaji, *Appl. Phys. A* **2022**, *128*, 475.
12. S. J. Saadoon, M. Jarosova, P. Machek, M. M. Kadhim, M. H. Ali, A. D. Khalaji, *J. Chin. Chem. Soc.* **2021**, 1-9.
13. S. Sehar, I. Naz, A. Rehman, W. Sun, S. S. Alhewairini, M. N. Zahid, A. Younis, *App. Organomet. Chem.* **2020**, e6069.
14. M. Vatanparast, L. Saeidi, *J. Mater. Sci. Mater. Electron.* **2018**, *29*, 7107-7113.
15. X. Yang, Y. Liu, J. Li, Y. Zhang, *Mater. Lett.* **2019**, *241*, 76-79.
16. S. Safat, F. Buazar, S. Albukhaty, S. Matroodi, *Sci. Rep.* **2021**, *11*, 14734.
17. D. Majumder, I. Chakraborty, K. Mandal, S. Roy, *ACS Omega* **2019**, *4*, 4243-4251.
18. S. P. Keerthana, R. Yuvakkumar, G. Ravi, P. Kumar, M. S. Elshikh, H. H. Alkhamis, A. F. Alrefaei, D. Valauthapillai, *Chemosphere* **2021**, *270*, 129498.
19. Z. Hammache, A. Soukeur, S. Omeiri, B. Bellal, M. Trari, *J. Mater. Sci. Mater. Electron.* **2019**, *30*, 5375-5382.
20. M. Punzi, F. Nilsson, A. Anbalagan, B. M. Svensson, K. Jonsson, B. Mattiasson, M. Jonstrup, *J. Hazard. Mater.* **2015**, *292*, 52-60.
21. K. Wang, A. A. Abdalla, M. A. Khaleel, N. Hilal, M. K. Kharisheh, *Desalination* **2017**, *401*, 190-205.
22. J. C. Cardoso, G. G. Bessegato, M. V. B. Zanoni, *Water Res.* **2016**, *98*, 39-46.
23. C. Byrne, G. Subramanian, S. C. Pillai, *J. Environ. Chem. Eng.* **2018**, *6*, 3531-3555.
24. G. Crini, E. Lichtfouse, *Environ. Chem. Lett.* **2019**, *17*, 145-155.
25. N. C. Cinperi, E. Ozturk, N. O. Yigit, M. Kitis, *J. Clean. Prod.* **2019**, *223*, 837-848.
26. A. E. Amoli, M. Masoumi, M. S. Baei, F. Babaei, G. F. Pasha, *J. Water Environ. Nanotechnol.* **20232**, *8*, 52-65.
27. N. V. Iyer, G. L. Agawane, A. Bhapkar, J. A. Kher, S. D. Bhame, *J. Water Environ. Nanotechnol.* **2023**, *8*, 23-33.
28. C. N. C. Hitam, A. A. Jalil, *J. Environ. Manag.* **2020**, *258*, 110050.
29. A. D. Khalaji, P. Machek, M. Jarosova, *Adv. J. Chem. A* **2021**, *4*, 317-326.
30. A. D. Khalaji, *Phys. Chem. Res.* **2022**, *10*, 473-483.
31. H. Yin, Y. Zhao, Q. Hua, J. Zhang, Y. Zhang, X. Xu, Y. Long, J. Tang, F. Wang, *Frontiers Chem.* **2019**, *7*, Article 58.
32. A. D. Khalaji, E. S. Zeinoddin, A. Ghorbani Khorshidi, A. Ghaffari, *Nanochem. Res.* **2023**, *8*, 278-286.
33. C. Wang, Z. Huang, *Chem. Lett.* **2015**, *44*, 1682-1684.
34. A. D. Khalaji, S. M. Mousavi, Z. Palamg Sangdevini, M. Jarosova, P. Machek, M. Dusek, *J. Sci. IRI.* **2021**, *32*, 213-219.
35. A. D. Khalaji, Z. Palang Sangdevini, S. M. Mousavi, M. Jarosova, P. Machek, *Asian J. Nanosci. Mater.* **2021**, *4*, 137-146.
36. M. Li, H. Liu, S. Pang, P. Yan, M. Liu, M. Ding, B. Zhang, *Nanomaterials* **2021**, *11*, 2650.
37. M. M. Sajid, T. Alomayri, *J. Taibah Uni. Sci.* **2022**, *16*, 1192-1201.
38. V. C. Karade, S. B. Parit, V. V. Dawkar, R. S. Devan, R. J. Choudhary, V. V. Kedge, N. V. Pawar, J. H. Kim, A. D. Chougale, *Heliyon* **2019**, *5*, e02044.
39. S. Taghavi Fardood, F. Moradnia, S. Moradi, R. Forootan, F. Yekke Zare, M. Heidari, *Nanochem. Res.* **2019**, *4*, 140-147.
40. A. Lassoued, M. S. Lassoued, B. Dkhil, S. Ammar, A. Gadri, *Phys. E* **2018**, *97*, 328-334.
4. S. J. Saadoon, M. Jarosova, P. Machek, M. M. Kadhim, M. H. Ali, A. D. Khalaji, *J. Chin. Chem. Soc.* **2021**, *69*, 280-288.
42. A. D. Khalaji, M. Jarosova, P. Machek, K. Chen, D. Xue, *Scripta Mater.* **2020**, *181*, 53-57.
43. A. D. Khalaji, S. M. Mousavi, M. Jarosova, P. Machek, *J. Surf. Invest: X-ray, Synch. Neut. Tech.* **2020**, *14*, 1190-1193.
44. A. D. Khalaji, M. Soleymanifard, M. Jarosova, P. Machek, *Acta Phys. Slov.* **2020**, *137*, 1043-1045.
45 A. D. Khalaji, Z. Pazhand, K. Kiani, P. Machek, M. Jarosova, R. Mazandarani, *J. Mater. Sci: Mater. Elect.* **2020**, *31*, 11949-11954.
46. A. D. Khalaji, M. Jarosova, P. Machek, K. Chen, D. Xue, *J. Nanostruct.* **2020**, *10*, 607-612.

47. A. D. Khalaji, *Nanochem. Res.* **2020**, *5*, 148-153.
48. A. Rufus, N. Sreeju, D. Philip, *J. Phys. Chem. Solids* **2019**, *124*, 221-234.
49. A. Lassoued, M.S. Lassoued, B. Dkhil, S. Ammar, *Phys. E.* **2018**, *101*, 212-219.
50. J. Wang, X. Shao, Q. Zhang, G. Tian, X. Ji, W. Bao, *J. Mol. Liq.* **2017**, *248*, 13-18.
51. V. Barron, J. Banas, *J. Colloid. Interface Sci.* **1966**, *177*, 407-410.
52. C. Rochester, S. A. Topham, *J. Chem. Sep. Faraday Trans.* **1979**, *1*, 1073-1088.
53. E. Mccafferty, *Electrochim. Acta* **2010**, *55*, 1630-1837.